Polymer Journal (2022) 54:697–705
https://doi.org/10.1038/s41428-021-00609-5

ORIGINAL ARTICLE

Reconfigurable and NIR-responsive shape memory polymer containing bipheunit units and graphene

Jing Yang[1,2] · Junhui Gong[1,3] · Liming Tao[1,3] · Zhangzhang Tang[1,2] · Zenghui Yang[1] · Pengrui Cao[1,3] · Qihua Wang[1,3] · Tingmei Wang[1,3] · Heming Luo[2] · Yaoming Zhang[1,3]

Received: 4 September 2021 / Revised: 7 December 2021 / Accepted: 7 December 2021 / Published online: 21 January 2022

Abstract

A series of near-infrared (NIR)-responsive shape memory polymers based on biphenyl epoxy (BPEP/GR) were prepared by mixed amine thermal curing and photocuring with an iodized salt photoinitiator and aromatic ferrocene photosensitizer (IOD/FC) initiator. Differential scanning calorimetry (DSC), dynamic mechanical analysis (DMA), and tensile test results indicated that the addition of graphene to a biphenyl-containing epoxy resin matrix led to improvements in the transition temperature, strength, and shape memory properties. Shape recovery could be completed within a few seconds by NIR irradiation due to the high photothermal conversion efficiency of graphene. NIR laser irradiation promoted the activation and recombination of biphenyl units due to local heating. Thus, a reconfigured shape was obtained. This new reconfiguration method is expected to help realize the important application of BPEP/GR composites in the field of intelligent soft robots.

Introduction

Shape memory polymers (SMPs), which can undergo target shape/volume changes under external stimuli such as electricity [1], magnetism [2], heat [3], chemistry [4], light [5, 6], and so on, have attracted broad attention for realizing the functions of soft robots and artificial muscles. In particular, a light-responsive SMP can be remotely, instantaneously, and precisely triggered to perform shape changes. Generally, there are two strategies for fabricating light-responsive shape memory polymers: (1) The introduction of photoresponsive compounds that can undergo photochemical reactions, such as isomerized azobenzene and reversible cyclobutane formation of coumarin dimers, where the aggregate effects of the change in chemical bonds of the polymer are amplified and manifested in the form of a shape change; and (2) the incorporation of fillers with photothermal effects into the polymer matrix, including organic dyes [7], graphene [8, 9], carbon nanotubes [10], polydopamine nanoparticles [11], etc. In this case, the absorbed light energy can be rapidly converted into heat and transferred through the fillers to the matrix to trigger shape recovery. Due to its versatility and convenience, the second strategy is favored for developing various light-responsive SMPs. Near-infrared (NIR) light (with a wavelength range of 780 nm to 1400 nm) possesses high penetrability and low hazard and is recognized as a very promising photothermal source for light-responsive SMPs. Liang et al. [12] showed that adding 1 wt% sulfonated graphene sheets to polyurethane enables NIR light responsiveness, with a high incident energy density (0.40 J/g) enabling the material to generate a sufficiently powerful force for lifting objects.

The temperature induced by the photothermal effect can be controlled in a specific range, and it depends on both the matrix and photothermal filler. Significantly, a polymer matrix with an excellent shape memory effect (SME) and

Supplementary information The online version contains supplementary material available at https://doi.org/10.1038/s41428-021-00609-5.

✉ Heming Luo
luohm666@163.com

✉ Yaoming Zhang
yaomingzhang@licp.cas.cn

[1] Key Laboratory of Science and Technology on Wear and Protection of Materials, Lanzhou Institute of Chemical Physics, Chinese Academy of Sciences, Lanzhou 730000, China

[2] College of Petrochemical Technology, Lanzhou University of Technology, Lanzhou 730050, China

[3] Center of Materials Science and Optoelectronics Engineering, University of Chinese Academy of Sciences, Beijing 100049, China

suitable transition temperature (T_r) is essential for realizing NIR-responsive SMPs. Shape memory epoxy resin (SMEP) with high mechanical strength and tunable T_r is considered a good SMP matrix, and it has been studied widely as a deployment structure. Although the use of rigid epoxy resin (EP) usually limits application of SMEP as an actuator [13], the rigidity issue can be overcome by varying the monomers or curing agents. By reasonable selection of a curing agent, a biphenyl unit containing epoxy resin can be tailored as a liquid crystal elastomer that possesses high mechanical strength, fracture toughness, and reversible SME. Due to the specific liquid crystalline feature, Kessler et al. [14] synthesized smectic liquid crystalline epoxy resin with good SME by using a biphenyl epoxy monomer and aliphatic carboxylic acid curing agent, which reached an elongation at break of 200%.

In comparison to controlled polymerization, it is well known that fast radical polymerization results in random polymer conformations that are fixed while crosslinking occurs [15]. Through special posttreatment, the frozen polymer conformation can be realigned; thus, the shape is reconfigured. Photo-polymerization is usually carried out in the form of rapid polymerization. For instance, EP curing under UV light with a photoinitiator composed of diaryliodonium salts and different photosensitizers can be completed in several hundred seconds [16]. In addition, incorporation with ferrocene (FC) with diaryliodonium salts as a cationic photoinitiator combination can shift the effective absorption to the UV range and initiate fast photopolymerization of epoxy resins [17, 18]. Chen et al. [19] found that the combination of FC/IOD effectively promoted a hybrid polymerization of bisphenol A epoxy resin (DGEBA) under a halogen lamp. The authors also proposed that hybrid polymerization can improve the performance of light-cured polymers. Therefore, we expected to observe a reconfigurable shape memory effect by using hybrid polymerization of a biphenyl unit containing epoxy resin.

In this paper, biphenyl-containing epoxy resin (BPEP) with an excellent shape memory effect was prepared by mixing the curing process of aromatic amine thermal curing and photocuring with a FC/IOD initiator. Adding graphene (GR) to the SMEP matrix enables BPEP/GR with NIR-triggered shape recovery properties. The deformed BPEP/GR with a 3D structure rapidly recovered to a 2D film by remote NIR irradiation. Furthermore, because the crystal structure of the biphenyl unit can be regulated through rapid polymerization, thermal treatment is applicable. The activation and recombination of the biphenyl units and the NIR responsiveness results in the self-folding behavior of BPEP/GR under NIR laser irradiation. It is also recognized as a reconfigured permanent shape, which can be recovered under a thermal stimulus. This work provides a novel strategy for reconfiguring the permanent shape of SMPs, and it is expected to widen the application of this type of material.

Experimental section

Materials

4,4′-Dihydroxybiphenyl, epichlorohydrin, and m-xylylenediamine (MXDA) were purchased from Saen Chemical Technology (Shanghai) Co., Ltd, China, Chengdu Cologne Chemicals Co. Ltd., and J&K Scientific Ltd., respectively. Isopropanol, toluene, N,N-dimethylacetamide (DMAC), and other solvents were purchased from Rionlon Bohua (Tianjin) Pharmaceutical & Chemical Co. Ltd. Graphene (SE1430) was purchased from The Sixth Element (Changzhou) Materials Technology Co., Ltd. All chemical reagents were used as received. Bis(4-phenyl) iodonium hexafluorophosphate (IOD), (η6-benzene) (η5-cyclopentadienyl) iron hexafluorophosphate (FC) were prepared according to previous reports [20, 21]. The epoxy monomer diglycidylether of biphenyl (DGEBP) was synthesized by the reaction of 4,4′-dihydroxybiphenyl and epichlorohydrin [22, 23]. The detailed synthetic procedure is provided in the Supporting Information.

Preparation of biphenyl epoxy resin/graphene composites (BPEP/GR)

The synthetic procedure of BPEP/GR is shown in Scheme 1. The photoinitiator combination of IOD (2 wt%)

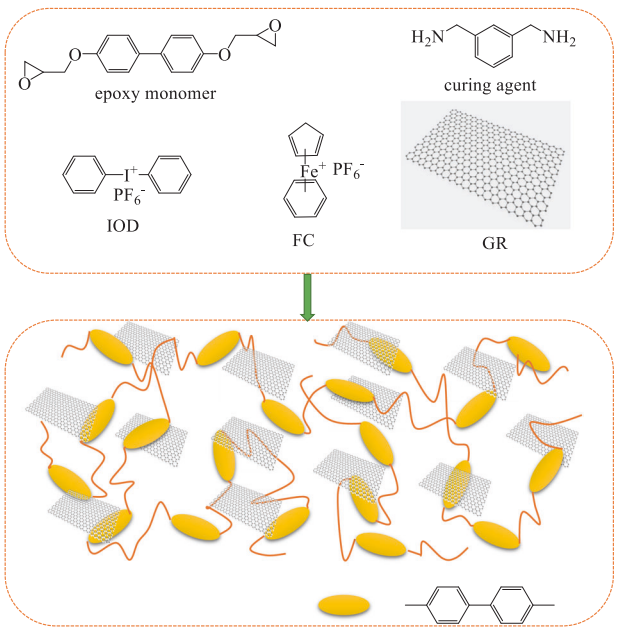

Scheme 1 The synthesis procedure of BPEP/GR films

and FC (1 wt%) was used to assist the hybrid polymerization of BPEP. Briefly, DGEBP and MXDA with a molar ratio of amine/epoxy = 0.68 were dissolved in DMAC at 100 °C, and then, the photoinitiator combination was added and mixed together. Next, the mixture was poured into a Teflon mold and irradiated under a 365 nm high-pressure mercury lamp to carry out curing and solvent evaporation. The cured films were further dried in a vacuum oven at 55 °C to further evaporate the solvent until a constant weight was achieved. NIR-responsive polymer films (BPEP/GR) were prepared by adding varying contents of graphene (0.5 wt%, 1 wt%, 1.5 wt%, 2 wt%) to BPEP before photoirradiation followed by the same curing procedure.

Characterization

A Bruker S V70 Fourier transform infrared spectrometer (FTIR) was used to verify the photocuring process. FTIR spectra within the wavenumber range of 3750–600 cm^{-1} were obtained by testing either the free-standing film or the solution coated on a KBr sheet. Bruker nuclear magnetic resonance spectroscopy (NMR, 400 MHz) was used to perform chemical structure analysis, and the deuterium-substituted reagent DMSO-d_6 was used as the solvent. A Shimadzu UV1800 UV–Vis spectrophotometer was used to measure the absorption spectra of the photoinitiators and photosensitizers and to analyze their photolysis reactions. Methanol was selected as the solvent, and the scanning wavelength range was 200–600 nm. The morphology of the BPEP/GR composites in liquid nitrogen was tested by field emission scanning electron microscopy (FESEM, Tescan Mira3, Czech Republic). All samples were spray-coated with gold before testing. A portable thermal conductivity meter (TC3000E, XIATECH) was used to determine the thermal diffusivity of the films. The near-infrared response performance of BPEP/GR was tested using a near-infrared laser (NBET) and a near-infrared lamp (Philips, 250 W).

The thermal performance was investigated with a synchronous thermal analyzer (STA449F). The samples were heated from room temperature to 180 °C to remove the thermal histories. Afterward, the samples were cooled to −50 °C by liquid nitrogen followed by a second heating step from −50 °C to 180 °C, and the scanning speed was 5 °C min^{-1}. Each formulation was repeated at least 3 times to verify the uniformity of the sample. The glass transition temperature (T_g) was determined from the second heating scan. The mechanical properties were tested by a universal tensile testing machine (Shimadzu AD-X (5000 N)). The sample was cut into a dumbbell shape according to ISO 527-2/1BB. The testing speed was 5 mm min^{-1}. At least 5 samples were measured, and the values were averaged. The thermodynamic behavior of the samples was analyzed by a dynamic mechanical thermal analyzer (DMA 242 C, Netzsch). The data were collected within a temperature range of −20~200 °C, at a heating rate of 10 °C min^{-1}, and at a frequency of 1 Hz. The shape memory performance was evaluated by using a dynamic mechanical thermal analyzer (DMA 242C) in tensile mode (TMA), and the heating and cooling rate was set to 5 °C min^{-1}. The sample was cut into a size of 20 mm × 3 mm, and the thickness was approximately 0.1 mm. The test process is described as follows: First, the sample was heated to $T_g + 30$ °C, a constant force was applied to stretch the sample for 3 min, and then, the sample was cooled to 20 °C. Under force loading, the maximum strain reached at this state is denoted as ε_m. Second, the external force was unloaded after equilibrium at 20 °C, and this strain was named ε_u. Finally, the sample was heated to $T_g + 30$ °C again and maintained for 30 min in the stress-free form, with the sample contracting with a strain of ε_r. The shape fixity ratio (R_f) and shape recovery ratio (R_r) were calculated according to the following equations [24]:

$$R_f = \frac{\varepsilon_u(N)}{\varepsilon_m(N-1)} \times 100\% \quad (1)$$

$$R_r = \frac{\varepsilon_u(N) - \varepsilon_r(N)}{\varepsilon_u(N) - \varepsilon_r(N-1)} \times 100\% \quad (2)$$

where N is the number of DMA test cycles. In this study, four shape memory cycles were performed. The frozen stress in the film during the curing process leads to a lower R_r in the first cycle; thus, 2–4 shape memory cycles were used to calculate the average R_f and R_r.

Results and discussion

1. The physical and chemical properties and shape memory behavior of the BPEP/GR film

It has been reported that photo-polyaddition of epoxy-amine under visible light can be accelerated by a photosensitizer/iodonium [19, 25]. Thus, a combination of FC/IOD is expected to work as a photoinitiator to assist the polyaddition of DGEBP and MXDA under UV light irradiation. As shown in Figs. 1a, b, the IOD absorption is located in the wavelength range of 200–300 nm. With increasing UV light irradiation time, the intensity at the peak observed at 227 nm decreases but the intensity at the peak observed at 290 nm increases, referring to the photodegradation of IOD. Whereas the absorption of aromatic ferrocene photosensitizer ranges from 200–500 nm, the absorption peaks at 390 nm and 450 nm correspond to the *d-d* transition of FC, and the strong absorption observed at 240 nm belongs to the π - π transition of the benzene ring in the closed-loop conjugated system [17, 18]. The synergistic effect induced

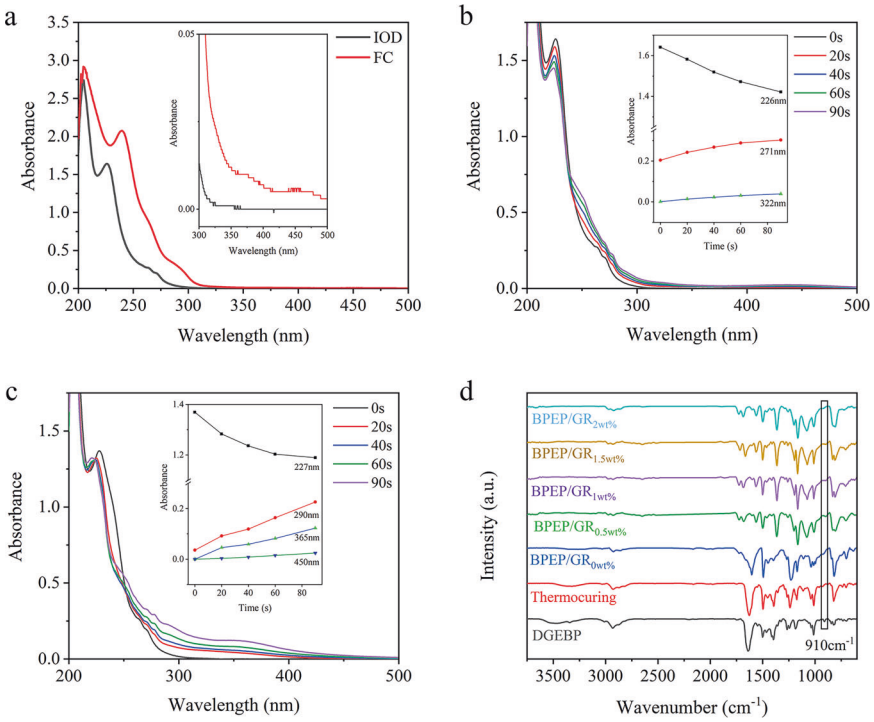

Fig. 1 **a** UV–Vis absorption spectra of IOD and FC. **b** Effect of irradiation time on the absorption spectrum of IOD. **c** Effect of irradiation time on the absorption spectrum of FC/IOD. **d** FTIR spectra of DGEBP and BPEP/GR

by the combination of FC/IOD was observed. Figure 1c shows a wide absorption range of 300–500 nm, and the absorption intensity is extended and enhanced in comparison with IOD. The photodegradation of IOD yields a strong protonic acid (HPF_6) and active Lewis acid, which are favored for the polyaddition of epoxy/amine [19]. As shown in Fig. 1d, the FTIR spectra show the disappearance of the characteristic oxirane peak at 910 cm^{-1} due to C-O stretching after irradiation with 365 nm UV light for 15 min. The FTIR spectrum is the same as that obtained after 1 h of thermal curing, which indicates that the curing time is shortened by using the hybrid curing system.

Based on our previous work [26], BPEP can present an excellent shape memory effect (SME). Therefore, the incorporation of photothermal graphene enables one to tune the thermomechanical properties due to crosslinking between GR and BPEP. Figure 2a shows the loss factor (Tan δ) of BPEP/GR over a broad temperature range from 50 °C to 90 °C. Increasing GR content results in the differentiation of Tan δ toward higher temperatures. Trace amounts of hydroxyl, carboxyl and epoxy groups were detected in pure GR (Fig. S3), which can react with the BPEP matrix and yield additional crosslinking that limits the movement of the polymer chain, leading to an increase in the T_g of BPEP/GR [27]. In addition, the formation of a crosslinked structure avoids the agglomeration of graphene in the polymer matrix, as demonstrated in Fig. S4 such that a small amount of added graphene (0.5 wt%) could be homogeneously dispersed in the BPEP matrix. The wide loss factor curve is mainly due to the random cross-linking structure generated by the mixed curing of amine and photoacid ions. Figure 2c shows the second heating differential scanning calorimetry (DSC) curves of BPEP/GR. The glass transition temperature of BPEP/GR changes with increasing GR content, which is consistent with the DMA results. The detailed information is summarized in Table 1.

The mechanical properties of the BPEP/GR films were measured by a universal tensile testing machine at room temperature. The tensile strength and elastic modulus of the pure BPEP polymer are 30 MPa and 2.4 GPa, respectively. Adding 0.5 wt% GR enhanced the tensile strength and elastic modulus of BPEP/GR to 53 MPa and 3.5 GPa, respectively. This result was attributed to the cross-linking reaction between graphene and the polymer matrix, which enhanced the interfacial compatibility. Therefore, we conclude that the addition of GR plays a role in the strengthening phase in the polymer matrix, thereby promoting the overall mechanical properties. However, due to the additional crosslinking, the elongation at break of BPEP/GR was significantly decreased from 17% to 6%. The tensile strength and elastic modulus of BPEP/GR decreased with increasing graphene content from 0.5 wt% to 2 wt%, which may be related to the partial local agglomeration of GR, resulting in weakened continuity of the polymer matrix [28, 29]. The details of the mechanical properties are summarized in Table 1.

The significant changes observed for the storage modulus E′ from 2.8 GPa to 26 MPa over the transition temperature suggest a promising SME and a high recovering stress (Fig. 2b) [30, 31]. Four shape memory cycles were

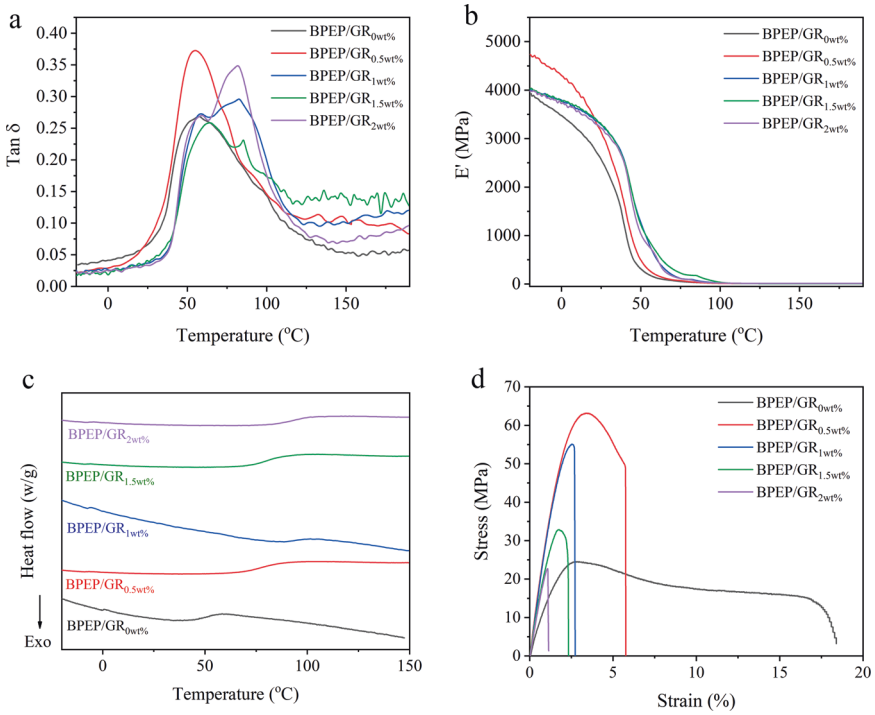

Fig. 2 **a** Loss factor (Tan δ) versus temperature curve of BPEP/GR films (**b**) The storage modulus curves of BPEP/GR films. **c** DSC curves of BPEP/GR. **d** Characteristic stress–strain curves of BPEP/GR

Table 1 Detailed information of the thermophysical, mechanical, and shape memory properties of BPER/GR

Films	T_g^a (°C)	T_g^b (°C)	E (MPa)	σ_b (MPa)	ε_b (%)	R_f (%)	R_r (%)
$BPER/GR_{0wt\%}$	51.3	57.3	2442.7 ± 181.1	30.2 ± 4.5	17.0 ± 8.1	99.5 ± 0.1	94.5 ± 1.9
$BPER/GR_{0.5wt\%}$	78.9	55.0	3477.1 ± 240.3	53.0 ± 2.9	5.7 ± 2.9	99.6 ± 0.1	95.7 ± 1.3
$BPER/GR_{1wt\%}$	88.6	82.5	3138.66 ± 455.8	34.5 ± 12.5	2.2 ± 0.8	99.4 ± 0.1	95.8 ± 3.8
$BPER/GR_{1.5wt\%}$	82.1	85.3	3284.4 ± 410.8	30.6 ± 7.0	2.3 ± 0.5	99.6 ± 0.1	98.0 ± 1.7
$BPER/GR_{2wt\%}$	93.1	83.4	3771.8 ± 577.6	26.0 ± 3.5	1.6 ± 0.6	99.5 ± 0.1	99.3 ± 1.1

[a, b]Glass transition temperature (T_g) determined from DSC and DMA measurements

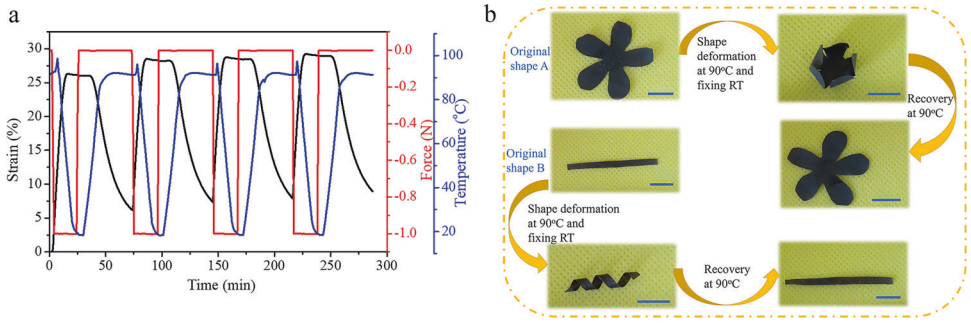

Fig. 3 **a** Shape memory cycles of BPEP/GR0.5wt% (**b**) Demonstration of the shape memory effect of $BPEP/GR_{0.5wt\%}$. Scale bar: 1 cm

performed by DMA to quantitatively evaluate the BPEP/GR shape memory properties, as shown in Fig. 3a. Shape fixity ratios above 99% and shape recovery ratios above 95% were obtained, and the specific data are shown in Fig. S5 and Table 1. Although the addition of GR led to confinement of the polymer chain movement, the recoverable strain reached approximately 20%. Moreover, the R_r of BPEP/GR gradually increased with increasing graphene content (Table 1 and Fig. S6). A small amount of graphene led to an increase in the strength of the polymer material, resulting in a large recovery strain. As shown in Fig. 3b, the thin film with a flower shape was folded at 90 °C and subsequently cooled to room temperature to fix the temporary shape, and heating at 90 °C enabled recovery of the unfolded film within 4 min. Similarly, the curled spiral could be fixed and recovered to a strip due to the SME.

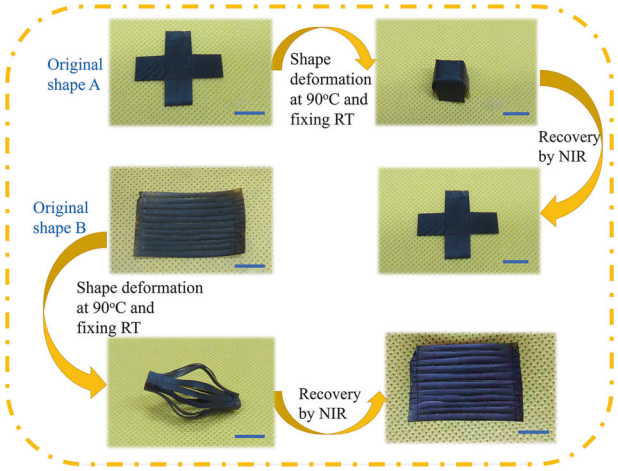

Fig. 4 NIR-triggered shape memory performance of BPEP/GR0.5wt% Scale bar: 1 cm

2. NIR responsiveness of BPEP/GR

Graphene is an effective photothermal conversion material that can be used to realize the conversion of light energy to heat when exposed to light. Adding GR to SMP endowed the composite with unique photoresponsiveness, and the photothermal energy further induced shape recovery. To verify the NIR-triggered shape memory effect of BPER/GR, a 2D film with a specific shape was deformed into temporary box and lantern shapes above the T_g, as shown in SI (Videos S1-S4) and Fig. 4. The 2D film was quickly recovered from the folding boxes and lanterns within a few seconds of NIR irradiation. The high photothermal property of GR and fast heating transfer in BPEP/GR allowed the temperature to increase and trigger rapid shape memory recovery. Fig. S7 shows the thermal conductivity coefficient for the BPEP/GR composite material, which increased linearly with increasing content of GR from 0.1722 to 0.2377; however, a high content of GR (2 wt%) resulted in a slight reduction in the thermal conductivity due to aggregation. Compared with that of pure BPEP, the increased thermal conductivity coefficient of BPEP/GR could assist heating diffusion to realize thermal shape memory [32]. In comparison to heating, NIR stimulation can realize remote control of shape recovery. In addition, instantaneous shape recovery shows wide potential application of well-defined actuators.

3. NIR-induced reconfigurable shape of BPEP/GR shape memory

Photothermal properties and rapid heat transfer are essential to realize the NIR responsive shape memory effect of BPEP/GR composites. The photothermal properties were evaluated by monitoring the temperature of a $BPEP/GR_{0.5wt\%}$ composite under NIR laser (808 nm) irradiation with tunable power. As shown in Fig. 5a, $BPEP/GR_{0.5wt\%}$ showed fast NIR responsiveness, and the temperature rapidly increased to a stable value after 20 s of irradiation. In addition, the maximum temperature obtained following NIR irradiation was positively correlated with the NIR laser current intensity, and tuning the current from 1 A to 1.3 A enabled adjusting the temperature from 60 °C to 180 °C. The effect of GR content on the photothermal properties was not significant under a fixed current intensity of 1.1 A, as shown in Fig. 5b. The temperature was stable within the range of 110 °C–140 °C when the GR content increased from 0.5 wt% to 2 wt%. Furthermore, the NIR irradiation-induced increase in temperature rapidly decreased to room temperature within approximately 30 s after switching off the light irradiation. The results indicate that the temperature can be increased above the T_g of BPEP/GR by NIR irradiation; therefore, NIR-controlled shape memory is expected to be observed.

The effect of NIR laser irradiation on the microstructure of BPEP/GR was investigated by XRD. The XRD patterns of $BPEP/GR_{0.5wt\%}$ before and after NIR laser irradiation for 30 s at a laser current intensity of 1.1 A show a change in microstructure. Figure 5d shows the Debye ring of the 2D WAXD data, while Fig. 5c was obtained by integrating the 2D WAXD patterns. The peaks observed at $2\theta = 19.6°$ ($d = 4.5$ Å) and $2\theta = 2.4°$ ($d = 36.1$ Å) correspond to ordered crystal structures due to the transverse stacking of biphenyl units. The abundant biphenyl units in BPEP could facilitate crystallization due to the strong π-π interactions between biphenyl groups, which is well known in liquid crystal elastomers [24, 31]. The POM micrograph (Fig. S8) also confirmed the crystallization of BPEP. In addition, the unique layered structure was attributed to the self-assembly of biphenyl intermediates during the mixed curing process due to π–π interactions [33]. The addition of a small amount of graphene had no effect on the crystal phase compared with the WAXD pattern of pure BPEP (Fig. S9). However, a new diffraction peak appeared at $2\theta = 10.9°$ ($d = 8.1$ Å) along with a weakening of the intensity of the peak observed at $2\theta = 19.6°$ ($d = 4.5$ Å) after NIR irradiation. NIR radiation induced a rapid temperature increase in the presence of graphene, which enabled the polymer chains to self-assemble into a higher-order structure.

In our previous study [26], the biphenyl structure and chemical structure formed by fast curing could be self-assembled into a compact structure by postheating-induced π-π interaction between biphenyl groups, such that a reconfigurable permanent shape could be tailored for this biphenyl-containing SMP. Analogously, the transformation of the crystalline phase could be used to tailor the BPEP with an adjustable shape memory performance. Due to the high photothermal conversion capacity of graphene, a high-power NIR laser can play the role of postheating to tune the

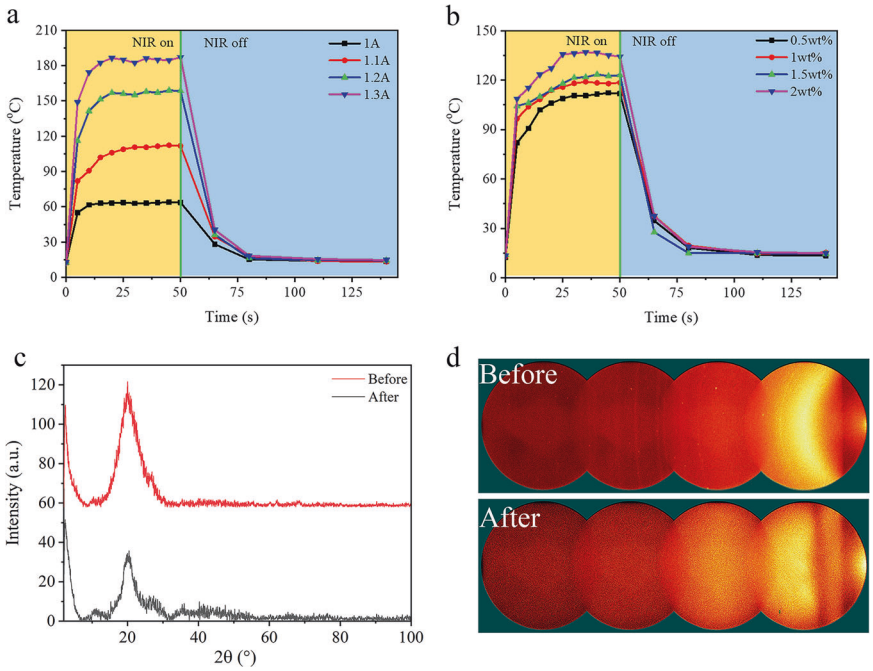

Fig. 5 **a** Effect of NIR laser intensity on the temperature of BPEP/GR. **b** Effect of GR content on the photothermal temperature of BPEP/GR under NIR laser irradiation. 1D WAXD patterns (**c**) and 2D WAXD patterns (**d**) of BPEP/GR0.5wt% before and after NIR irradiation, respectively

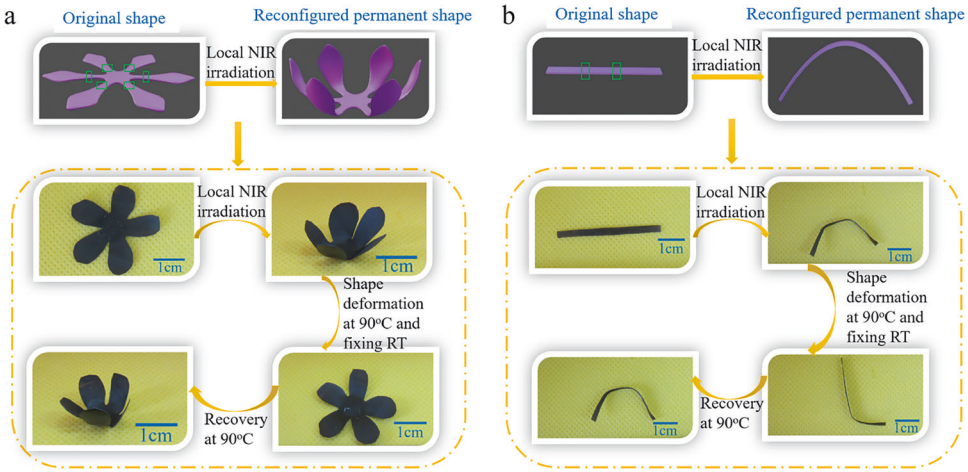

Fig. 6 Demonstration of NIR reconfigured permanent shape of shape memory polymer BPEP/$GR_{0.5wt\%}$; the current intensity was set to 1.1 A. **a** Reconfiguration of flower shape into flower bud as permanent shape through NIR irradiation. **b** Reconfiguration of strip shape into "n" shape as permanent shape through NIR irradiation

chemical structure of BPEP. As shown in Fig. 6, the BPEP/$GR_{0.5wt\%}$ film self-folded into a flower bud and a "n" shape when the marked region was irradiated by an 808 nm NIR laser. These shapes were stable even after removal of the laser irradiation. Then, the self-folded samples were heated at 90 °C and redeformed into a blooming flower and an "L" shape. Next, upon reheating these samples, the NIR programmed shape rather than the initial shape was recovered. Therefore, we speculate that NIR irradiation results in changes in the chemical structure, which induce reconfigurable permanent shape formation. On the one hand, the high local temperature of the irradiation region triggers the reorganization of the polymer segments due to the self-assembly of the biphenyl units. Rapid cooling can result in freezing of the new crystalline phase and the formation of a new structure. On the other hand, the light penetration is limited due to the absorption gradient from the irradiation side to the backside of the sample. Therefore, NIR irradiation induces self-folding, which is a new permanent shape for BPEP/GR. Similar to vitrimers [34–36] with dynamic covalent bonds that can remold permanent shapes, our work provides a new strategy for reconfigurable shape memory polymers.

Conclusions

In summary, we prepared a series of NIR-responsive biphenyl epoxy resin/graphene composite films. We verified the synergistic initiation between FC and IOD by UV–Vis absorption spectroscopy. The mechanical properties, transition temperature, and shape memory properties of

the composite films were controlled by adjusting the graphene content. BPEP/GR exhibits an excellent shape memory effect, with a shape fixity ratio exceeding 99% and a shape recovery ratio of 96%. A fast NIR-responsive shape recovery was obtained by adding graphene, and the high photothermal conversion efficiency of GR led to an increase in the temperature of BPEP/GR due to remote near-infrared irradiation. The activation and recombination of the biphenyl units can form a new structure to realize reconfiguration of the permanent shape for the shape memory material. This work provides a facile method for preparing NIR-responsive shape memory polymers, and the remote-controlled shape change broadens the application of this BPEP/GR composite. This reconfigurable method promotes the development of BPEP/GR composites for application in bionics and intelligent soft robots.

Author contributions The manuscript was written with contributions from all authors. All authors have given approval to the final version of the manuscript.

Funding The authors gratefully acknowledge financial support from the National Natural Science Foundation of China (51935012, 52005481), Key Research Program of Frontier Science, Chinese Academy of Science (QYZDJ-SSW-SLH056), One-Three-Five Strategic Planning of Chinese Academy of Sciences, and Key Research Program of the Chinese Academy of Sciences (Grant No. XDPB24).

Compliance with ethical standards

Conflict of interest The authors declare no competing interests.

Publisher's note Springer Nature remains neutral with regard to jurisdictional claims in published maps and institutional affiliations.

References

1. Lu H, Gou J, Leng J, Du S. Synergistic effect of carbon nanofiber and sub-micro filamentary nickel nanostrand on the shape memory polymer nanocomposite. Smart Mater Struct. 2011;20:035017.
2. Kaiser A, Winkler M, Krause S, Finkelmann H, Schmidt AM. Magnetoactive liquid crystal elastomer nanocomposites. J Mater Chem. 2009;19:538–43.
3. Xie T. Tunable polymer multi-shape memory effect. Nature. 2010;464:267–70.
4. Boothby JM, Kim H, Ware TH. Shape changes in chemoresponsive liquid crystal elastomers. Sens Actuat B-Chem. 2017;240:511–8.
5. Lu XL, Zhang H, Fei GX, Yu B, Tong X, Xia HS, et al. Liquid-crystalline dynamic networks doped with gold nanorods showing enhanced photocontrol of actuation. Adv Mater. 2018;30:1706597.
6. Li JJ, Zhou X, Liu ZF. Recent advances in photoactuators and their applications in intelligent bionic movements. Adv Opt Mater. 2020;8:202000886.
7. Ge F, Yang R, Tong X, Camerel F, Zhao Y. A multifunctional dye-doped liquid crystal polymer actuator: light-guided transportation, turning in locomotion, and autonomous motion. Angew Chem Int Ed. 2018;57:11758–63.
8. Wei W, Zhang Z, Wei J, Li X, Guo J. Phototriggered selective actuation and self-oscillating in dual-phase liquid crystal photonic actuators. Adv Opt Mater. 2018;6:1800131.
9. Yang Y, Zhan W, Peng R, He C, Pang X, Shi D, et al. Graphene-enabled superior and tunable photomechanical actuation in liquid crystalline elastomer nanocomposites. Adv Mater. 2015;27:6376–81.
10. Li C, Liu Y, Lo C-W, Jiang H. Reversible white-light actuation of carbon nanotube incorporated liquid crystalline elastomer nanocomposites. Soft Matter. 2011;7:7511–6.
11. Li Z, Yang Y, Wang Z, Zhang X, Chen Q, Qian X, et al. Polydopamine nanoparticles doped in liquid crystal elastomers for producing dynamic 3D structures. J Mater Chem A. 2017;5:6740–6.
12. Liang JJ, Xu YF, Huang Y, Zhang L, Wang Y, Ma YF, et al. Infrared-triggered actuators from graphene-based nanocomposites. J Phys Chem C. 2009;113:9921–7.
13. Kumar KSS, Biju R, Nair CPR. Progress in shape memory epoxy resins. React Funct Polym. 2013;73:421–30.
14. Li YZ, Pruitt C, Rios O, Wei LQ, Rock M, Keum JK, et al. Controlled shape memory behavior of a smectic main-chain liquid crystalline elastomer. Macromolecules. 2015;48:2864–74.
15. Saed MO, Terentjev EM. Siloxane crosslinks with dynamic bond exchange enable shape programming in liquid-crystalline elastomers. Sci Rep. 2020;10:6609.
16. Crivello JV, Liu SS. Photoinitiated cationic polymerization of epoxy alcohol monomers. J Polym Sci Pol Chem. 2000;38:389–401.
17. Wang T, Chen JW, Li ZQ, Wan PY. Several ferrocenium salts as efficient photoinitiators and thermal initiators for cationic epoxy polymerization. J Photochem Photobiol A. 2007;187:389–94.
18. Wang T, Li Z, Zhang Y, Lu M. Synthesis and photoactivity of novel cationic photoinitiators: (η6-Diphenylmethane) (η5-cyclopentadienyl) iron hexafluorophosphate and (η6-benzophenone) (η5-cyclopentadienyl) iron hexafluorophosphate. Prog Org Coat. 2009;65:251–6.
19. Chen Y, Jia XQ, Wang MQ, Wang T. A synergistic effect of a ferrocenium salt on the diaryliodonium salt-induced visible-light curing of bisphenol-A epoxy resin. RSC Adv. 2015;5:33171–6.
20. Beringer FM, Drexler M, Gindler EM, Lumpkin CC. Diaryliodonium salts .1. Synthesis. J Am Chem Soc. 1953;75:2705–8.
21. Beringer FM, Falk RA, Karniol M, Lillien I, Masullo G, Mausner M, et al. Diaryliodonium salts .9. The synthesis of substituted diphenyliodonium salts. J Am Chem Soc. 1959;81:342–51.
22. Sadafule DS, Raghuraman RN, Navale NG, Kumbhar CG, Panda SP. A photocrosslinkable vinyl polyester. J Macromol Sci-Chem. 2006;25:121–6.
23. Belmonte A, Lama GC, Gentile G, Fernandez-Francos X, De la Flor S, Cerruti P, et al. Synthesis and characterization of liquid-crystalline networks: toward autonomous shape-memory actuation. J Phys Chem C. 2017;121:22403–14.
24. Miao JT, Ge M, Peng S, Zhong J, Li Y, Weng Z, et al. Dynamic imine bond-based shape memory polymers with permanent shape reconfigurability for 4D printing. ACS Appl Mater Interfaces. 2019;11:40642–51.
25. Garra P, Graff B, Schrodj G, Morlet-Savary F, Dietlin C, Fouassier J-P, et al. Ultrafast epoxy–amine photopolyaddition. ACS Macromol. 2018;51:10230–6.
26. Yang J, Tao LM, Cao PR, Yang ZH, Zhang XR, Wang QH, et al. Biphenyl containing shape memory epoxy resin with post-heating adjustable properties. Macromol Mater Eng. 2021;306:2100185.
27. Chen G-K, Wu K, Zhang Q, Shi Y-c, Lu M-G. Dual-responsive shape memory and thermally reconfigurable reduced graphene oxide-vitrimer composites. Macromol Res. 2019;27:526–33.

28. Kamaraj M, Dodson EA, Datta S. Effect of graphene on the properties of flax fabric reinforced epoxy composites. Adv Compos Mater. 2019;29:443–58.
29. Fan YH, Yu SW, Wang HM, Yao YH, Wang Y, Wang CH. Study on preparation and properties of graphene reinforced epoxy resin composites. IOP Conf Ser: Mater Sci Eng 2019;634:012044.
30. Yu XJ, Zhou SB, Zheng XT, Guo T, Xiao Y, Song BT. A biodegradable shape-memory nanocomposite with excellent magnetism sensitivity. Nanotechnology. 2009;20:235702.
31. Xie T, Xiao XC. Self-peeling reversible dry adhesive system. Chem Mater. 2008;20:2866–8.
32. Chen L, Li WB, Liu YJ, Leng JS. Nanocomposites of epoxy-based shape memory polymer and thermally reduced graphite oxide: Mechanical, thermal and shape memory characterizations. Compos Part B-Eng. 2016;91:75–82.
33. Lehmann W, Skupin H, Tolksdorf C, Gebhard E, Zentel R, Kruger P, et al. Giant lateral electrostriction in ferroelectric liquid-crystalline elastomers. Nature. 2001;410:447–50.
34. Montarnal D, Capelot M, Tournilhac F, Leibler L. Silica-like malleable materials from permanent organic networks. Science. 2011;334:965–8.
35. Cao Y, Zhang JT, Zhang DD, Lv Y, Li J, Xu YT, et al. A novel shape memory-assisted and thermo-induced self-healing boron nitride/epoxy composites based on Diels-Alder reaction. J Mater Sci. 2020;55:11325–38.
36. Chakma P, Konkolewicz D. Dynamic covalent bonds in polymeric materials. Angew Chem Int Ed. 2019;58:9682–95.